10.2478/msr-2014-0002

Liquid Film Thickness Estimation using Electrical Capacitance Tomography

Ziqiang Cui, Chengyi Yang, Benyuan Sun, Huaxiang Wang

Tianjin Key Laboratory of Process Measurement and Control,
School of Electrical Engineering & Automation, Tianjin University, Tianjin 300072, China

In air/oil lubrication systems, the flow parameters, *e.g.*, flow pattern, liquid film thickness, and air/oil flow rate, are of great importance to the transportation efficiency. In most cases, the on-going two-phase flow is annular flow with the oil moving along the tube wall and the air travelling at high speed in the center. This usually results in the formation of a thin oil film, the thickness of which is a key parameter determining the efficiency of the lubrication system. As the oil film thickness of the on-going air/oil flow varies dynamically, there is actually no applicable method for a non-intrusive test. In this paper, the use of electrical capacitance tomography (ECT) to investigate the air/oil flow has been studied. Capacitance measurements are made from an externally mounted electrode array in a non-invasive and non-intrusive manner. Both average and distributed oil film thicknesses can be calculated from the reconstructed ECT images. Simulation and experimental results show that the ECT technique can provide satisfactory results of online oil film thickness estimation.

Keywords: Electrical capacitance tomography, liquid film thickness, two phase flow.

1. INTRODUCTION

LIQUID FILM occurs very often in industrial applications with thicknesses that may range from below 10 μm to above 5 mm. For instance, during the operation of air/oil lubrication system, a thin film of lubrication oil forms along the wall of the transportation tube, in which the distribution and composition of the oil film are critical for the lubrication efficiency [1], [2]. Thin films are also present when a gas or vapor and a liquid flow through a pipe together. The liquid distribution and film thickness are the most important parameters in modeling the flows where liquid film is present. In the past, most film measurement methods focused on water related applications, *i.e.* taking advantage of its electrical conductive properties. Such methods include the needle-contact method and electrical conductance method. However, different methods became necessary when non-conductive fluids, *i.e.* oil, are involved. Electrical capacitance measurements have attracted much interest throughout a long period, primarily due to the fact that capacitance can be measured on non-conductive fluids, eliminating one of the significant constraints of the needle contact method and electrical conductance method. However, such methods are only capable of making measurement at a certain point of the flow. When liquid distribution is needed for flow modeling and controlling, the conventional methods will no longer work.

ECT is a tomographic tool that uses capacitance measurements obtained at the periphery of the investigated vessel or pipe to map the permittivity distribution within its sensing region. It has been widely used in multi-phase flow measurement in oil, chemical and power industries [3]-[5]. Dual-mode measurements, *i.e.* ECT and other measurement techniques, are also proposed for better resolution images [6].

In ECT applications, the sensor diameter is usually above 100 mm [7], [8]. Applications of small sensor diameters, *i.e.* less than 10 mm, are also introduced. T. A. York et al. have presented a solution to the application of ECT in micro-scale flow measurement, in which the hole diameter to be measured is only 500 μm [9], [10]. J. T. Li et al. have employed the ECT technique in a thermosyphon system with a dedicated sensor [11]. In these applications, the sensors are intrusive, *i.e.* in direct contact with the on-going fluids. However, it is not desirable to employ an intrusive sensor since it may interrupt the flow and affect the measurement accuracy. Therefore, the intended use of ECT for online measurement of liquid film requires a design of a non-intrusive sensor that is suitable for the flows in a small diameter pipe/tube. High precision capacitance measuring circuit is required when the sensor dimension gets smaller. It should be noted that ECT image resolution is not uniform over its sensing region and increases from the center towards the tube wall. This could be an actual benefit of using ECT for oil film measurement as it is typically near tube walls.

In this paper, the use of ECT technique for online measurement of liquid film in a small diameter pipe/tube is investigated. Special treatments have been applied to the ECT sensor and the measuring circuit to enhance its capability of small diameter pipe/tube measurement. The proposed method is a practical and simple technology for liquid film measurement, which could provide online liquid distribution as well as the liquid film thickness.

2. METHODS

In consideration of the small diameter of the tested pipe/tube, the ECT sensor design and the capacitance measuring circuits have to be reconsidered. It is a common sense that it is not likely to extract a clear gas-liquid interface from the raw ECT images. Therefore, a method has been developed for calculating the liquid film thickness from the raw measurements or ECT images.

A. Sensor design

The number of electrodes is a key parameter in designing the ECT sensor. In most applications, the sensor diameter is between 50 and 1000 *mm*. More measurements can be made from a sensor of more electrodes. Therefore, there are usually 12 or 16 electrodes in the ECT sensor in order to achieve better axial resolution of reconstructed images. Such sensor can be made from copper sheet. The fabrication tolerance of 1 % will not significantly affect measurement accuracy. In this application, however, the tube diameter is too small to employ a complex sensor configuration. Therefore, the ECT sensor is composed of 8 electrodes.

For reliable and accurate measurement, a sensor consisting of flexible printed circuit (FPC) electrode and aluminum alloy enclosure has been designed and implemented, as shown in Fig.1. The electrode array is screened and protected by an aluminum alloy enclosure, as shown in Fig.1.a). The sensor cross-sectional is illustrated in Fig.1.b). For easy installation, the 8 electrodes are divided into two groups, each containing four electrodes, as shown in Fig.1.c).

a) The installed ECT sensor with metal cover.

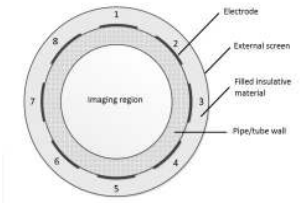

b) Sensor cross-sectional.

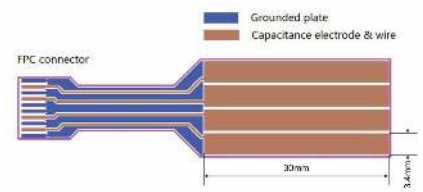

c) The FPC sensor (10 *mm* diameter, 4 electrodes included).

Fig.1. The ECT sensor.

For a small diameter ECT sensor, the capacitance measurements are more likely to be affected by mechanical vibration. The so-called 'negative sensing region' effect becomes significant in a smaller sensor, especially when external electrodes are used. It means that the increase of equivalent permittivity in such region probably causes a decrease in capacitance measurements, especially for the neighboring-electrode capacitances.

In implementing the circuit, the impact of mutual coupling capacitances between channels has been taken into consideration, as schematically shown in Fig.2. As the coupling capacitance C_p is in parallel with the measured capacitance C_x, it will contribute to the base value of the measurement and take up the effective measurement range of the circuit. Considering that the ac based c/v circuit is immune to stray capacitance, it would be a good practice to transform a coupling capacitance into stray capacitances, *i.e.* by laying a grounded track.

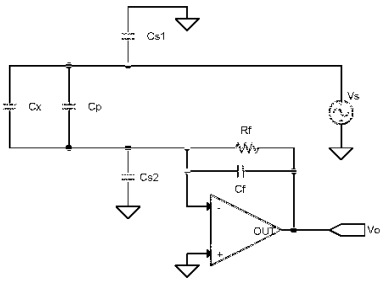

Fig.2. The coupling capacitance.

B. Small capacitance measurement

In ECT, measuring capacitance accurately is a challenging procedure in itself, particularly with capacitance changes on the order 10 *fF* or less indicating oil film variation. In ac-based c/v circuit, the circuitry gain is determined by the feedback resistor R_f and capacitor C_f in the following form

$$V_o \approx -\frac{C_x}{C_f} V_i \tag{1}$$

where C_x is the measured capacitance, V_i and V_o are the amplitudes of the input and output voltage signals, respectively.

It can be noted that C_f should be decreased to increase the circuitry gain. However, the shunt parasitic capacitances that exist on the PCB set a lower limit for equivalent feedback capacitance. Therefore, post-amplifiers are needed to increase the overall gain.

The number of independent measurements in ECT is determined by

$$m = C_n^2 = n(n-1)/2 \tag{2}$$

where n is the number of the electrode. For n = 8, m = 28.

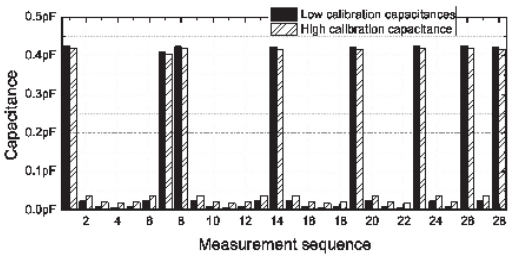

Fig.3. Low and high calibration capacitance data.

Low and high calibration data are obtained for the sensor filled with low and high permittivity materials, respectively. As can be seen from Fig.3., in most cases high calibration

data are greater than the low calibration data. However, for the neighboring-electrode capacitances, it is the exact opposite. This is due to the so-called 'negative sensitivity region' phenomenon. This characteristic can be harmful to the image reconstruction quality. Therefore, the neighboring-electrode capacitances are removed from the measurement set, which contains only 20 capacitances. By removing such data point, the dynamic range of the measuring circuits can be rationally reduced, thus achieving better resolution for low capacitances.

The normalized capacitances are usually used instead of the raw data in ECT image reconstruction, which is determined by the following formula.

$$\eta = \frac{C_m - C_l}{C_h - C_l} \tag{3}$$

where η is the normalized capacitance. C_m, C_l and C_h are the measured capacitance, low and high calibration capacitance, respectively.

Considering that the measured capacitances are small, it is necessary to make compensation to the raw measurements. To achieve this, a reference capacitor is employed to perform calibration before measurement. The reference capacitor was measured by an impedance analyzer (Agilent 4294A). The reference capacitor is used to derive true value of the measured capacitance. By applying the reference to each measuring channel, the measuring channels can be calibrated, thus improving channel consistence. The calibration procedure is carried out regularly for long term stability of the measurement system.

C. Estimation of oil film thickness

The dynamic characteristic of oil flow makes it difficult to perform online estimation of the film thickness. To estimate the oil film thickness, the relationship between the oil concentration and oil film thickness is established.

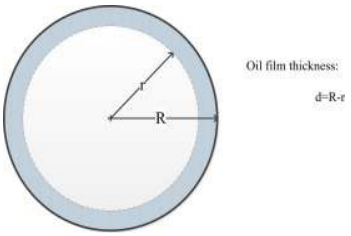

Fig.4. Oil film in the tube.

It is assumed that oil film is uniformly distributed around the wall, as shown in Fig.4. Therefore, the following equation can be used to describe the relationship between the reconstructed images and oil concentration.

$$\rho = 1 - \frac{\pi r^2}{\pi R^2} = \frac{1}{P}\sum_{i=1}^{P} g_i \tag{4}$$

where ρ is the oil concentration at the sensor cross-sectional, g_i is the equivalent permittivity of the i^{th} pixel of the ECT image and P is the number of the pixel.

The oil film thickness $d = R - r$. By combining it with (4), the oil film thickness can be obtained.

$$d = R\left(1 - \sqrt{1 - \frac{1}{P}\sum_{i=1}^{P} g_i}\right) \tag{5}$$

Because the uniform distribution is only a special case, it is necessary to find a more general solution to the oil film thickness. To achieve this, the sensor cross-sectional is equally divided into k sectors, as shown in Fig.5. The angle of each sector is θ.

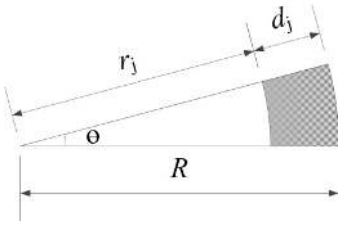

Fig.5. Oil film thickness in a sector.

For each sector, equations (6), (7) and (8) can be derived:

$$\rho_j = 1 - \frac{\pi r_j^2}{\pi R^2} = \frac{1}{P_j}\sum_{i\in\Omega_j} g_i \tag{6}$$

$$d_j = R\left(1 - \sqrt{1 - \frac{1}{P_j}\sum_{i\in\Omega_j} g_i}\right) \tag{7}$$

$$d_j = R - r_j \tag{8}$$

where ρ_j is the oil concentration of the j^{th} sector, d_j and r_j are the oil film thickness and radius of the air phase of the j^{th} sector, respectively. Ω_j is the region of the j^{th} sector and P_j is the number of the pixel within Ω_j.

The following equations are needed to understand the relations between ρ_j and ρ_j,

$$\rho = \sum_{j=1}^{k} \rho_j \tag{9}$$

$$P = \sum_{j=1}^{k} P_j \tag{10}$$

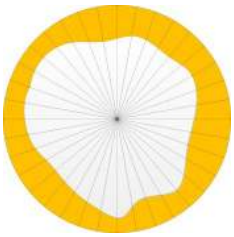

a) The basics of the proposed method.

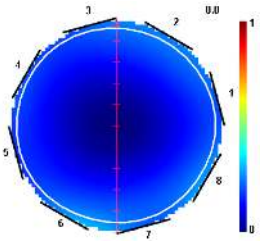

b) The image from the tomographic software (the white line indicating the oil film interface).

Fig.6. Oil film distribution.

By dividing the cross-sectional into *k* sectors, a set of oil film thicknesses can be obtained to represent the oil film distribution, as shown in Fig.6.

3. Results and Discussion

A. Numerical simulation

Numerical simulation method, *i.e.* finite element method (FEM), is employed to evaluate the proposed method. FEM simulations of different oil film thicknesses have to be carried out to determine the inter-electrode capacitances. To facilitate the simulation process, *i.e.* using a MATLAB code to automatically conduct the simulation process, the model is appropriately simplified, as shown in Fig.7. The simulation models can be simplified because the three parts, *i.e.* tube wall, lubrication oil and the filled insulating material, are of similar value in permittivity (2.7~3.5). Therefore, these parts are merged into one during simulation. In the simulation, the relative permittivity of the high permittivity parts is set to 3, and the relative permittivity of air is set to 1. This simplification also leads to a reduction in the element number. Considering that hundreds of different oil film thicknesses are to be included in the simulation, the simulation can be a tedious process.

By applying excitation voltage to an electrode and connecting other electrodes to ground, the electric potential distribution $\varphi(x,y)$ can be determined by FEM. The inter-electrode capacitances can be obtained using the following equation,

$$C = -\frac{1}{V_E}\oint_{\partial\Omega_M}\varepsilon(x,y)\nabla\varphi(x,y)d\tau \qquad (11)$$

where $\partial\Omega_M$ is the boundary of the measuring electrode, V_E is the electric potential of the excitation electrode, and $\varepsilon(x,y)$ is the permittivity distribution.

It usually can be derived that thicker oil film will result in an increase in the measured capacitance. However, the inter-electrode capacitances are not always in the parallel-plate form. In the simulation, the range of the oil film thickness is set to (0, 400 μm), *i.e.* (0, 0.1) of the internal diameter 4 *mm*. And four inter-electrode capacitances, *i.e.* $C_{(E1,E2)}$, $C_{(E1,E3)}$, $C_{(E1,E4)}$ and $C_{(E1,E5)}$, are plotted against oil film thickness, which are obtained from the 4 *mm* internal diameter tube. Taking the reciprocity of capacitance measurement and sensor shape into account, these capacitances can represent all possible electrode combinations.

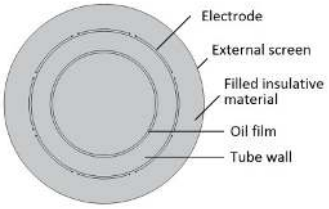

a) Original model.

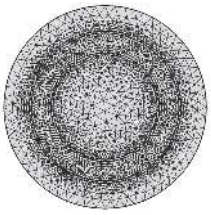

b) The mesh grid for the original model (5158 elements).

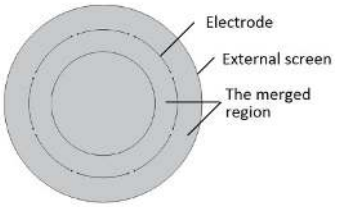

c) Simplified model.

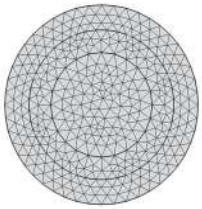

d) The mesh grid for the simplified model (690 elements).

Fig.7. The FEM models and their mesh grid.

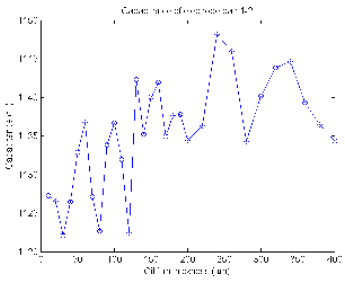

a) $C_{(E1,E2)}$

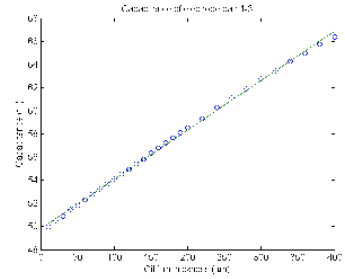

b) $C_{(E1,E3)}$

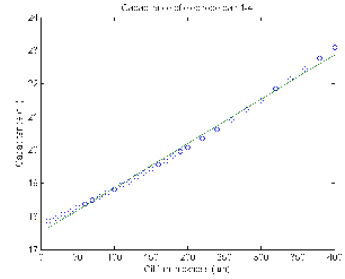

c) $C_{(E1,E4)}$

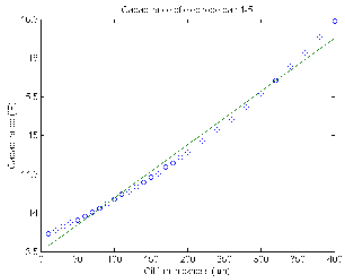

d) $C_{(E1,E5)}$

Fig.8. Inter-electrode capacitances for tube of 4 *mm* internal diameter.

As can be seen from Fig.8., the neighboring-electrode capacitance $C_{(E1,E2)}$ does not increase or decrease accordingly as the oil film thickness increases. This phenomenon is due to the existence of the 'negative sensing region'. Besides, all other capacitances present good linear relationships between the capacitance and oil film thickness. Least square method based linear fit ($C = ax + b$) is performed on $C_{(E1,E3)}$, $C_{(E1,E4)}$ and $C_{(E1,E5)}$, where a is the slope and b is the intercept. Detailed parameters are listed in Table 1.

As shown in Fig.8., the data sets can be readily approximated with its linear fit. It can also be found that the slope a is small, *i.e.* 0.0426, 0.0134 and 0.0069 $fF/\mu m$. Therefore, it would not be a reliable and robust method to estimate the oil film thickness with such raw data.

Table 1. The linearized curve-fitting parameters for three inter-electrode capacitances.

Inter-electrode capacitance	**Linear fitting parameters**	
	a ($fF/\mu m$)	B (fF)
C(E1, E3)	0.0426	49.8265
C(E1, E4)	0.0134	17.5186
C(E1, E5)	0.0069	13.5053

Table 2. The reconstructed images of uniformly distributed oil film.

Inverse algorithm	**Oil film thickness(μm)**			
	10	100	200	400
The simulation phantom	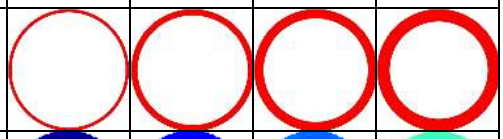			
LBP	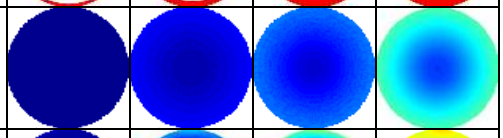			
TSVD	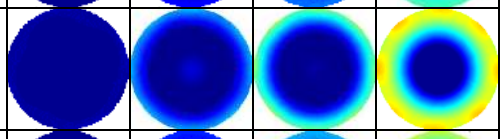			
Tikhonov Regularization	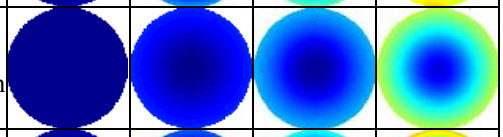			
Landweber Pre-iteration	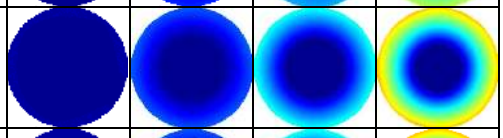			
Newton-Raphson Pre-iteration	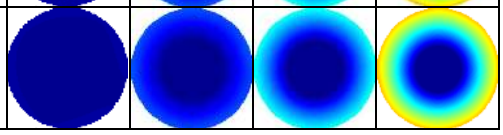			

Another possible method is to use reconstructed image for oil film estimation, which takes all measurements into account. It can provide better reliability and requires no excessive performance on the measuring circuit. As image reconstruction algorithm plays a key role in determining the permittivity distribution [13]-[15], a number of image reconstruction algorithms, *i.e.* LBP, TSVD, Tikhonov regularization, Landweber pre-iteration and Newton-Raphson pre-iteration, have been tested for comparative study.

As depicted in Table 2., the reconstructed images obtained from the aforementioned five algorithms are presented for the oil film thicknesses of 10, 100, 200 and 400 μm. The ECT images are always diffuse, *i.e.* no clear interface between the gas and liquid phases. Non-linear algorithms may provide better image quality, *i.e.* smaller transition area at the phase interface. However, it is still not applicable to distinguish the different phases by applying a threshold to the images because the image reconstruction is inherently ill-posed and under-determined.

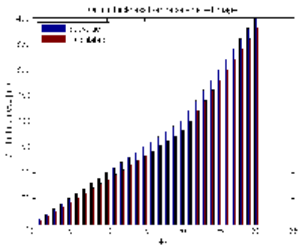

a) The set value *vs.* the calculated value.

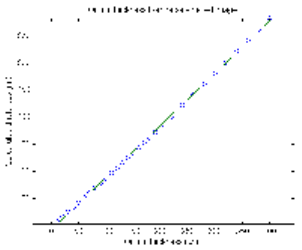

b) The linear fit of the calculated value.

Fig.9. The results of LBP algorithm.

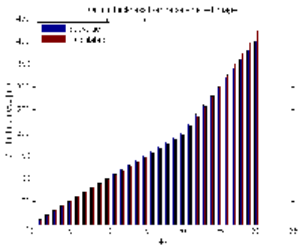

a) The set value *vs.* the calculated value.

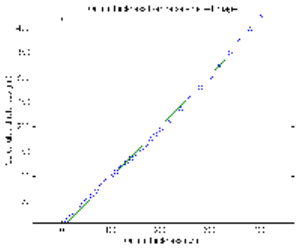

b) The linear fit of the calculated value.

Fig.10. The results of TSVD algorithm.

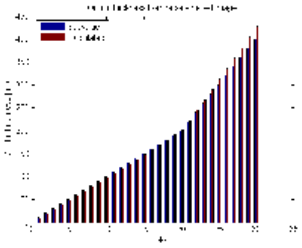

a) The set value *vs.* the calculated value.

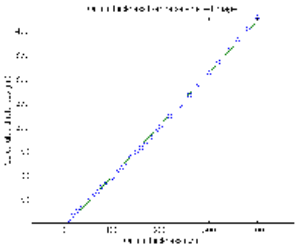

b) The linear fit of the calculated value.

Fig.11. The results of Tikhonov regularization algorithm.

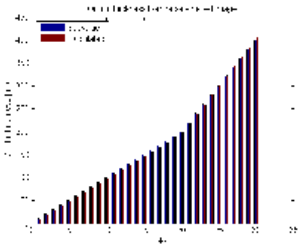

a) The set value *vs.* the calculated value.

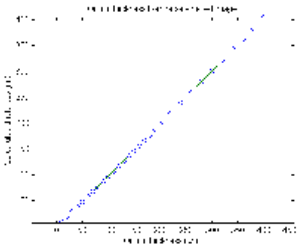

b) The linear fit of the calculated value.

Fig. 12. The results of Landweber pre-iteration algorithm.

This method is applied to the raw images, and the results are shown in Fig.9. ~ Fig.13. The linearized curve fitting parameters are listed in Table 3. for quantitative evaluation. The slope a for each curve fitting is close to 1, *i.e.* 0.9551, 1.0323, 1.0721, 1.0164 and 1.0154, which implies that the calculated values are in good accordance with the real values. It can also be concluded that the different image reconstruction algorithms have little impact on the accuracy of the proposed method. Even with the simplest algorithm, *i.e.* LBP, the results are comparable with those of other iterative algorithms. This phenomenon can be explained by that this method takes all 20 capacitance measurements, rather than one measurement, into account to obtain one result. Therefore, it is more likely to remove the errors caused by measurement instability.

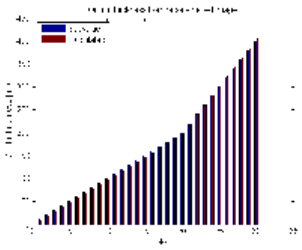

a) The set value *v.s.* the calculated value.

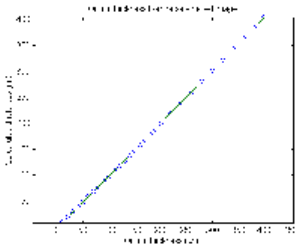

b) The linear fit of the calculated value.

Fig.13. The results of Newton-Raphson algorithm.

Table 3. The linearized curve-fitting parameters for the oil film thicknesses from the 5 algorithms.

Algorithm	Linearized curve-fitting parameters	
	a	*b*
LBP	0.9551	-6.6254
TSVD	1.0323	-4.9179
Tikhonov Regularization	1.0721	-8.8182
Landweber pre-teration	1.0164	-4.0369
Newton-Raphson pre-iteration	1.0154	-3.3239

B. Online test

Online experiments are also carried out. The ECT measurement system in this application is an FPGA based data acquisition system [16]. In this ECT system, most functions as required by ECT are implemented with digital signal processing method rather than analog method. The signal-to-noise ratio is evaluated to be above 60 *dB*. The experiments are carried out on a lubrication system, in which small amount of lubrication oil is driven by the compressed air. When the lubrication system is running, the oil is driven by the air and forms an annular flow. When the air supply is off, the oil stops running and begins to settle to the bottom. The tomographic images and oil film distribution are shown in Fig.14.

The phase interface calculated using the proposed method is plotted using a white line in the ECT image. ECT images are not likely to present a sharp phase interface indicating the oil film distribution. Case I shows the uniformly distributed oil film when the lubrication system is working. The corresponding bar graphs present values of film thickness in each sector. While the ECT images give a global view of the oil distributions, the bar graph can provide oil film thickness in all 36 sectors, which offers quantity controlling the lubrication process.

The film thickness variation in a specific sector can be extracted and plotted against time. Four oil film thicknesses, *i.e.* at the top, bottom, left and right side of the tube, are considered. The lubrication oil is intermittently supplied by a pump and blown by the compressed air. Different oil supply conditions, *i.e.* frequency and oil volume, can result in lubrication efficiency diversity, as shown in Fig.15. In Fig.15.a) and b), the oil feeding intervals are 40 s and 12 s, respectively. It can be found that smaller intervals of oil feeding lead to an overall thicker oil film.

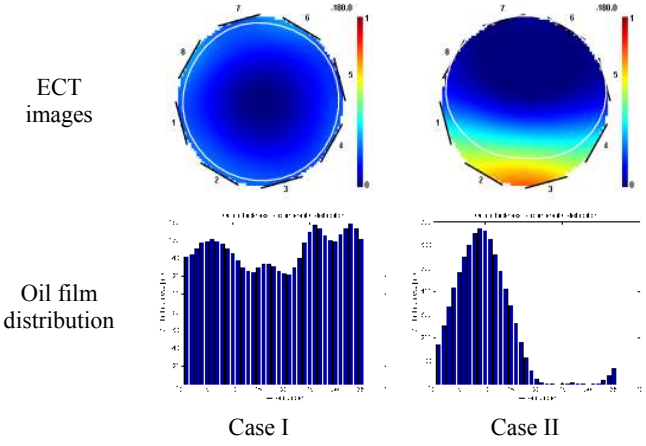

Fig.14. Reconstructed images of on-going air/oil flows

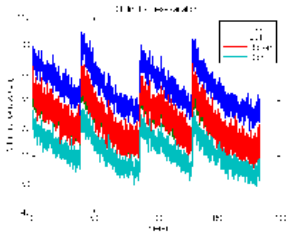

a) 40 s

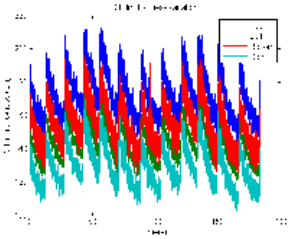

b) 12 s

Fig.15. Oil film variations of different feeding intervals.

4. CONCLUSIONS

This paper presents the simulation and experimental results of the ECT system for the estimation of oil film thickness in the air/oil flows. The results show that ECT has the potential to provide both qualitative and quantitative parameters of the air/oil flows, *e.g.*, flow pattern, oil concentration and oil film thickness.

The FPC based 8-electrode ECT sensor is designed and implemented to facilitate the measurement on the investigated small diameter tube. It has been proved that the ECT sensor fabricated using FPC material can be made as small as 4 *mm* I.D. As compared with other methods to fabricate a small diameter sensor, the FPC sensor is easy to use and has no interference on the investigated flow. As the size of the ECT sensor was reduced, some problems should be paid more attentions to. For example, in an industrial environment many factors, *e.g.*, mechanical vibration, power instability and electromagnetic interference, can lead to measurement failure.

Two methods are evaluated for estimating the liquid film thickness. The use of raw capacitance measurement to estimate the thickness is straightforward, but its performance is limited by the capacity of capacitance measuring circuit. Therefore, it is not likely to provide robust and accurate results. In contrast, the use of ECT images to calculate the oil film thickness involves the image reconstruction process, which is computation intensive and not so straightforward as compared with the aforementioned method. However, this method takes all measurements into account, thus is able to provide more robust and accurate results. It can also be concluded that this method has little requirements on the image reconstruction algorithm. Even with the LBP algorithm, it is capable to provide satisfactory results. Recently, more sophisticated algorithms like the nonlinear inversion technique and the fuzzy clustering method have been developed, which were proved to be efficient in ECT reconstruction to reveal complicated permittivity patterns[17], [18]. Future work will focus on using such advanced image reconstruction algorithms to achieve better results. It can be concluded that the use of the ECT technique to estimate the oil film thickness is an applicable and robust method, which also features the ability to provide online distributed oil film thicknesses.

ACKNOWLEDGMENTS

The authors would like to thank the financial support from Natural Science Foundation of China (Grant Nos. 61201350), the Doctoral Fund of the Ministry of Education of China (Grant Nos. 20120032120088) and Innovation Foundation of Tianjin University.

REFERENCES

[1] Wu, Ch.-H., Kung, Y.-T. (2005). A parametric study on oil/air lubrication of a high-speed spindle. *Precision Engineering*, 29 (2), 162-167.

[2] Höhn, B.-R., Michaelis, K., Otto, H.-P. (2009). Minimised gear lubrication by a minimum oil/air flow rate. *Wear*, 266 (3), 461-467.

[3] Ismail, I., Gamio, J.C., Bukhari, S.F.A., Yang, W.Q. (2005). Tomography for multi-phase flow measurement in the oil industry. In *Flow Measurement and Instrumentation*, 16 (2-3), 145-155.

[4] Marashdeh, Q. (2006). *Advances in electrical capacitance tomography*. Dissertation, Ohio State University.

[5] Li, Y., Yang, W., Xie, C., Huang, S., Wu, Z., Tsamakis, D., Lenn, Ch. (2013). Gas/oil/water flow measurement by electrical capacitance tomography. *Measurement Science and Technology*, 24 (7), 2013, 074001.

[6] Hjertaker, B.T., Maad, R., Johansen, G.A. (2011). Dual-mode capacitance and gamma-ray tomography using the Landweber reconstruction algorithm. *Measurement Science and Technology*, 22 (10), 104002.

[7] Yang, W.Q. (2010). Design of electrical capacitance tomography sensors. *Measurement Science and Technology*, 21 (4), 042001.

[8] Cai, R., Zhang, Y., Li, Q., Meng, A. (2013). Tracing the motion of a large object in a fluidized bed using electrical capacitance tomography. *Flow Measurement and Instrumentation*, 33, 1-9.

[9] Evans, I., Somerville, A., York, T.A. (1999). A sensing circuit for micro-capacitance tomography. In *1st World Congress on Industrial Process Tomography*, 14-17 April 1999. Virtual Centre for Industrial and Process Tomography (VCIPT), 395-401.

[10] York, T.A., Phua, T.N., Reichelt, L., Pawlowski, A., Kneer, R. (2006). A miniature electrical capacitance tomograph. *Measurement Science and Technology*, 17 (8), 2119.

[11] Liu, S., Li, J.T., Chen, Q. (2007). Visualization of flow pattern in thermosyphon by ECT. *Flow Measurement and Instrumentation*, 18 (5), 216-222.

[12] Yang, W.Q., York, T.A. (1999). New AC-based capacitance tomography system. *IEE Proceedings Science Measurement and Technology*, 146 (1), 47-53.

[13] Yang, W.Q., Spink, D.M., York, T.A., McCann, H. (1999). An image-reconstruction algorithm based on landweber's iteration method for electrical-capacitance tomography. *Measurement Science and Technology*, 10 (11), 1065.

[14] Wang, H.X., Wang, C., Yin, W.L. (2004). A pre-iteration method for the inverse problem in electrical impedance tomography. *IEEE Transactions on Instrumentation and Measurement*, 53 (4), 1093-1096.

[15] Yang, W.Q., Peng, L.H. (2003). Image reconstruction algorithms for electrical capacitance tomography. *Measurement Science and Technology*, 14 (1), R1.

[16] Cui, Z.Q., Wang, H.X., Chen, Z.Q., Xu, Y.B., Yang, W.Q. (2011). A high-performance digital system for electrical capacitance tomography. *Measurement Science and Technology*, 22 (5), 055503.

[17] Smolik, W. (2010). Fast forward problem solver for image reconstruction by nonlinear optimization in electrical capacitance tomography. *Flow Measurement and Instrumentation*, 21 (1), 70-77.

[18] Yue, S.H., Wu, T., Pan, J., Wang, H.X. (2013). Fuzzy clustering based ET image fusion. *Information Fusion*, 14 (4), 487-497.

Received September 5, 2013.
Accepted January 23, 2014.